Membrane deformable mirror for adaptive optics: performance limits in visual optics

Enrique J. Fernández and Pablo Artal

Laboratorio de Optica, Departamento de Física, Universidad de Murcia,
Campus de Espinardo (Edificio C),
30071 Murcia, Spain
enriquej@um.es; pablo@um.es

Abstract: The performance of a membrane deformable mirror with 37 electrodes (OKO Technologies) is studied in order to characterize its utility as an adaptive optics element. The control procedure is based on knowledge of the membrane's response under the action of each isolate electrode, i.e., the influence functions. The analysis of the mathematical techniques to obtain the control matrix gives useful information about the surfaces that are within the device's range of production, thus predicting the best performance of the mirror. We used a straightforward iterative algorithm to control the deformable membrane that permits the induction of surfaces in approximately four iterations, with an acceptable level of stability. The mirror and the control procedure are tested by means of generating Zernike polynomials and other surfaces. The mirror was incorporated in an adaptive optics prototype to compensate the eye's aberration in real time and in a closed loop. Double-pass retinal images with and without aberration correction were directly recorded in a real eye in order to evaluate the actual performance of the adaptive optics prototype.

OCIS codes: (010.1080) Adaptive optics; (350.4600) Optical engineering; (330.4460) Ophthalmic optics; (330.5370) Physiological optics

References and links

1. W. B. Bridges, P. T. Brunner, S. P. Lazzara, T. A. Nussmeier, T. R. O'Meara, J. A. Sanguinet, and W. P. Brown Jr., "Coherent optical adaptive optics techniques," Appl. Opt. **13**, 291-298 (1974).
2. J. W. Hardy, J. Feinleib, and J. C. Wyant, "Real time phase correction of optical imaging system," presented at the topical meeting on Optical Propagation through Turbulence, Boulder, Colorado, July 9-11 (1974).
3. N. Hubbin and L. Noethe, "What is adaptive optics?" Science **262**, 1345-1484 (1993).
4. M. S. Smirnov, "Measurement of the wave aberration in the human eye," Biophysics **6**, 776-794 (1961).
5. A. W. Dreher, J. F. Bille, and R. N. Weinreb, "Active optical depth resolution improvement of the laser tomographic scanner," Appl. Opt. **28**, 804-808 (1989).
6. P. Artal and R. Navarro, "High-resolution imaging of the living human fovea: measurement of the intercenter cone distance by speckle interferometry," Opt. Lett. **14**, 1098-1100 (1989).
7. J. Liang, D. R. Williams, and D. T. Miller, "Supernormal vision and high-resolution retinal imaging through adaptive optics," J. Opt. Soc. Am. A. **14**, 2884-2892 (1997).
8. F. Vargas-Martin, P. Prieto, and P. Artal, "Correction of the aberrations in the human eye with liquid crystal spatial light modulators: limits to the performance," J. Opt. Soc. Am. A. **15**, 2552-2562 (1998).
9. H. J. Hofer, P. Artal, B. Singer, J. L. Aragón, and D. R. Williams, "Dynamics of the eye's wave aberration," J. Opt. Soc. Am. A. **18**, 497-506 (2001).
10. E. J. Fernández, I. Iglesias, and P. Artal, "Closed-loop adaptive optics in the human eye," Opt. Lett. **26**, 746-748 (2001).
11. H. Hofer, L. Chen, G. Y. Yoon, B. Singer, Y. Yamauchi, and D. R. Williams, "Improvement in retinal image quality with dynamic correction of the eye's aberrations," Opt. Express **8**, 631-643 (2001), http://www.opticsexpress.org/abstract.cfm?URI=OPEX-8-11-631.
12. M. L. Plett, P. R. Barbier, and D. W. Rush, "Compact adaptive optical system based on blind optimization and micromachined membrane deformable mirror," Appl. Opt. **40**, 327-330 (2001).

#2380 - $15.00 US Received April 10, 2003; Revised April 25, 2003

13. E. S. Claflin and N. Bareket, "Configuring an electrostatic membrane mirror by least square fitting with analytically derived influence functions," J. Opt. Soc. Am. A **3**, 1833-1839 (1986).
14. D. Dayton, S. Restaino, J. Gonglewski, J. Gallegos, S. McDermott, S. Browne, S. Rogers, M. Vaidyanathan, and M. Shilko, "Laboratory and field demonstration of low cost membrane mirror adaptive optics system," Opt. Commun. **176**, 339-345 (2000).
15. L. Zhu, P.-C. Sun, and Y. Fainman, "Aberration-free dynamic focusing with a multichannel micromachined membrane deformable mirror," Appl. Opt. **38**, 5350-5354 (1999).
16. R. J. Noll, "Zernike polinomials and atmospheric turbulence, " J. Opt. Soc. Am. **66**, 207-211 (1976).
17. W. H. Press, S. A. Tekolsky, W. T. Vetterling, and B. P. Flannery, *Numerical Recipes in C*, 2nd ed. (Cambridge U. Press, New York, 1992).
18. G.-M. Dai, "Modal wave-front reconstruction with Zernike and Karhunen–Loève functions," J. Opt. Soc. Am. A **13**, 1218-1225 (1996).
19. P. Artal, I. Iglesias, N. Lopez-Gil, and D. G. Green, "Double-pass measurements of the retinal image quality with unequal entrance and exit pupils sizes and the reversibility of the eye's optical system," J. Opt. Soc. Am. A. **12**, 2358-2366 (1995).
20. G. Vdovin and P. M. Sarro, "Flexible mirror micromachined en silicon," Appl. Opt. **34**, 2968-2972 (1995).
21. C. Paterson, I. Munro, and J. C. Dainty, "A low cost adaptive optics system using a membrane mirror," Opt. Express **6**, 175-185 (2000), http://www.opticsexpress.org/abstract.cfm?URI=OPEX-6-9-175.
22. P. M. Prieto, F. Vargas-Martín, S. Goelz, and P. Artal, "Analysis of the performance of the Hartmann–Shack sensor in the human eye," J. Opt. Soc. Am. A **17**, 1388-1398 (2000).
23. E. J. Fernández, S. Manzanera, P. Piers, and P. Artal, "Adaptive optics visual simulator," J. Refract. Surg. **18**, S634-S638 (2002).

1. Introduction

A variety of devices for wave-front correction have been developed since the early days of adaptive optics (AO) [1-3]. Initially this technology was used mainly in astronomy to compensate the effects of atmospheric turbulence in images from large telescopes and in military applications. In the context of ophthalmic applications, Smirnov [4] first suggested the idea of correcting the aberrations of the eye in the early 1960s, probably independently from the previous ideas of application in astronomy. More recently, the use of a segmented mirror to correct astigmatism [5] and a speckle interferometry technique [6] were some of the antecedents for current applications of AO in ophthalmic applications. In the past 10 years, static corrections of the ocular aberrations were demonstrated in different laboratories by use of both deformable mirrors [7] and liquid-crystal spatial light modulators [8]. However, owing to the dynamic nature of the ocular aberration [9], real-time closed-loop aberration correction is actually required for obtaining a near to perfect compensation of the aberrations. In this direction, real-time AO systems for the eye that use deformable mirrors were recently reported [10,11].

Deformable mirrors have become the most widely used correcting elements in AO. The main advantages of these mirrors are probably their reflective nature, which allows for low loss of radiant energy flow, and its achromaticity, as opposed to liquid-crystal modulators. This makes the mirrors the preferred correcting devices in astronomical applications and also, although to a lesser extent, in visual optics applications, where the intensity of the light needs to be low to meet safety standards. There are a variety of deformable mirrors types, which are usually classified according to the performance in the deformation of their surfaces. Segmented mirrors, compounded by a number of mirrors whose movements are independent of one another, monolithic mirrors, and bimorph mirrors have been widely used. Within the monolithic class, electrostatic membrane mirrors have been one of the most employed types, probably owing to their moderate cost and reasonably good performance. Operation of the electrostatic mirrors is based on the induction of different voltages to the set of electrodes underneath the membrane causing the desired deformation over the mirrored surface, which remains at a constant voltage and is generally grounded. The main practical problem in employing this type of deformable mirror is the control procedure for selecting the set of voltages driving the mirror to the desired shape. Several control approaches have been proposed such as blind algorithms converging toward the final surface [12] and procedures based on a theoretical estimation of the membrane's behavior [13], although the

#2380 - $15.00 US Received April 10, 2003; Revised April 25, 2003

most widely used method is the one based on the successive measurement of the incoming wave front after reflection on the deformable mirror [14,15], permitting an iterative actuation over the membrane in closed loop to obtain the desired mirror shape.

In this manuscript, we describe a complete procedure to evaluate both theoretically and experimentally the limits of this type of deformable mirror to generate the desired wave front. Although this is a general approach, we will show results of the mirror operating in an AO prototype for correcting aberrations in the human eye. The paper is organized as follows. In Section 2 the matrix inversion method by singular-value decomposition (SVD) and its applications in the mirror's control are explained. In our methods, the practical use of the membrane mirror together with the experimental setup to test the mirror's capabilities is described. Section 3 shows the theoretical and experimental results for the mirror's performance and demonstrates the device for ocular aberration correction.

2. Theory

The procedure for controlling the electrostatic deformable membrane mirror used the previously measured influence functions. These functions are the responses of the membrane to the action of one particular isolated electrode. The set of functions can be grouped into the so-called influence functions matrix (IFM). Then we obtain the surface of the membrane as the response to a given set of voltages applied in the electrodes, assuming that the process is linear, by simple matrix multiplication:

$$IFM * \vec{V} = \vec{S}\,, \tag{1}$$

where vector **V** is the set of *k* squared voltages applied to each electrode (**V** = [v^2_1 v^2_2 ... ... v^2_k]) and **S** is the surface of the mirror expressed in terms of an expansion of Zernike's polynomials Z_j [16]:

$$\vec{S} = \begin{bmatrix} a_1 & a_2 & \dots & \dots & a_m \end{bmatrix};\ S = \sum_{j=1}^{m} a_j Z_j\,. \tag{2}$$

Equation (2) provides a procedure for controlling the surface of the mirror. The inverse of matrix IFM, the control matrix (CM), relates the desired surface, as vector of the Zernike coefficients to the required voltages by

$$CM * \vec{S} = \vec{V}\,. \tag{3}$$

Usual matrix inversion requires both nonsingular and square matrices. The IFM, however, does not ensure any of these characteristics. The mirror CM can be obtained by pseudoinversion of matrix IFM, by use of the SVD method. This permits the pseudoinversion of every matrix [17].

In addition, the set of surfaces that the mirror can exactly reproduce are obtained by use of SVD. They are functions associated with nonzero singular values in the decomposition of IFM. These can be understood as the spatial modes of the membrane. This is of practical importance, since any surface represented as a linear combination of the set of these modes will be perfectly produced by adequate voltages in the mirror's electrodes.

The effect of setting to zero a singular value in IFM before inversion is equivalent to removing one of the membrane modes, which can be convenient in some cases. A lower number of modes indicates a reduced capability to reproduce surfaces but also a more robust control of the mirror. Once the number of modes has been selected to handle the membrane, it is important to evaluate how the mirror will produce surfaces outside the domain of the control matrix. If a desired surface **s** is not in the domain of IFM, then Eq. (1) has no solution, but pseudoinversion will provide a vector of voltages **v′**, which produces a surface

#2380 - $15.00 US Received April 10, 2003; Revised April 25, 2003

s′ that belongs to the real domain of the matrix. In addition, this surface is the closest solution, in the least-squares sense, to the surface **s**. The obtained surface minimizes the parameter *r*, the residual, given by

$$r = \left| IFM \cdot \vec{v}' - \vec{s} \right| . \tag{4}$$

This procedure allows predicting, for any required surface, the most similar surface that can be actually produced by the mirror. The difference between the surfaces can be expressed through their Zernike polynomial expansions [18]. Under this representation, the residual is none other than the root mean square (rms) of the difference:

$$r = \left| \sum_i a'_i Z_i - \sum_j a_j Z_j \right| = \left| \sum_j \left(a'_j - a_j \right) \cdot Z_j \right| = \sqrt{\sum_j \left(a'_j - a_j \right)^2} = \text{rms} , \tag{5}$$

3. Experimental system

The experimental setup is shown in Fig. 1. It is based on an AO prototype for the eye [10]. A Hartmann–Shack wave-front sensor is placed optically conjugated with the membrane deformable mirror and with the entrance pupil of the whole system.

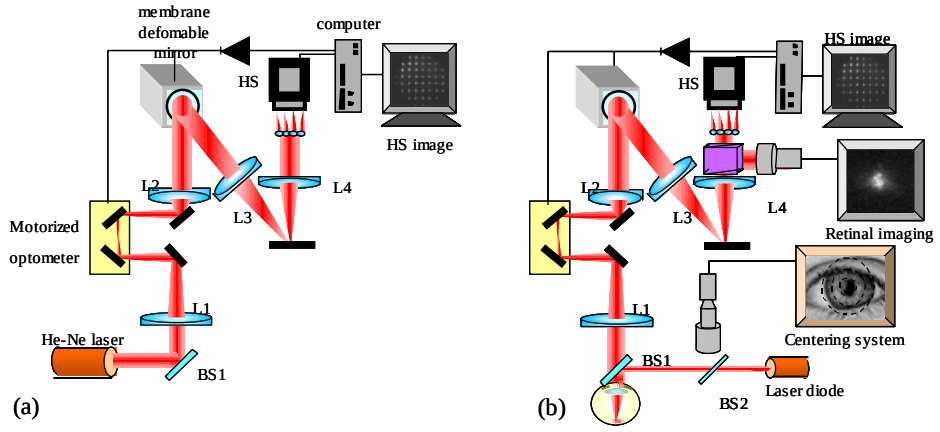

Fig. 1. (a) Experimental apparatus to test the deformable mirror. A reference beam is introduced in the system that measures the induced aberrations by means of a Hartmann–Shack wave-front sensor. (b) AO prototype for the human eye. Some modifications of the system permit the measurement and compensation of the ocular aberrations. Simultaneous recording of retinal images or visual task can be performed during the retrieval and correction of the wave.

Two achromatic doublets L1 and L2, with focal distances 120 and 200 mm, respectively, conjugate a 5.52-mm entrance pupil diameter over a 9.2-mm-diameter area on the deformable mirror. Another pair of achromatic doublets L3 and L4, with focal distances 200 and 100 mm, respectively, conjugate the membrane's selected zone (9.2-mm diameter) on the Hartmann–Shack sensor. The system incorporates a computer-controlled motorized optometer, to add the desired amounts of defocus. The Hartmann–Shack sensor consists of a microlens array (0.6-mm-square lenslets; focal length, 6.3 mm) and a CCD camera. The wave front is measured at a maximum rate of 25 Hz, limited by the acquisition camera time. For calibration of the system, a collimated He–Ne laser beam was used for illumination [Fig. 1 (a)]. For experiments with the eye, several components were added to the setup [Fig. 1 (b)]. A pigtailed infrared diode laser (780 nm) illuminated the eye (1.75-mm-diameter beam) to form a beacon source on the retina. An additional camera is used for alignment the eye with respect to the mirror and the sensor aperture. A cube beam splitter placed before the wave-

#2380 - $15.00 US
Received April 10, 2003; Revised April 25, 2003

front sensor allowed recording of retinal images simultaneously to the wave-front measurements [19].

The micromachined membrane deformable mirror was manufactured by OKO Technologies (Delft, The Netherlands) [20]. It consists of a chip with a silicon nitride membrane coated with aluminum with an effective mirrored diameter of 15 mm. Voltages applied to 37 control electrodes electrostatically drive the membrane shape. The membrane shape, $S(x,y)$, under a given pressure distribution $P(x,y)$, due to a voltage distribution $V(x,y)$ across the distance d, follows Poisson equation (6):

$$\nabla^2 S(x,y) = -\frac{P(x,y)}{T} = -\varepsilon_0 \frac{[V(x,y)]^2}{Td^2}, \tag{6}$$

where T is the membrane tension. The boundary condition is also required for solving Eq. (6). The membrane is coated with an evaporated layer of aluminum to make it reflective and conductive [21]. Digital boards provide 8-bit voltage control for the output channels, whereas the high-voltage drivers produce the final desired voltage value (range of 0–250 V) to each electrode.

To evaluate the mirror's performance, we used a system without the eye and for illumination used a plane wave front (produced by the He–Ne laser). After reflection of a plane wave in the mirror, the measured wave front is directly related with the mirror's surface (once the contributions of other components in the system are corrected).

Since the force between the membrane and the electrodes is attractive, the membrane can be pulled only toward its base. By biasing the mirror to a nonzero voltage, deformation in both directions can be induced. Values of 65% of the maximum voltage for the reference voltages are obtained by solution of Poisson equation (6), which describes the membrane behavior. Since we limited the operating range to 210 V for safety of the device, the reference value is 140 V. Experimental measurements of the membrane shape under 140 V in every electrode showed a 4-μm deflection. Since the specifications of the mirror predict a maximum deflection of 8 μm, the selected value for the bias appears to be adequate. Owing to the boundary conditions, the employed area of the mirror needs to be smaller than its complete metallic surface. Previous studies [22] with the same type of mirror demonstrated that the use of ~60 % of the membrane's diameter is the best choice for obtaining the maximum number of independent modes. We followed the same strategy here: the beam diameter on the mirror was set for all experiments to 9.2 mm, which represents 61 % of the membrane's total area.

The influence functions of the mirror were obtained by application of sequential voltages to each electrode during measurement of the produced wave front with the Hartmann–Shack sensor [23]. Some examples of these influence functions are shown in Fig. 2. The total area of the mirror and the electrode configuration are schematically presented. The inner red circle is the employed area on the mirror where the influence functions were measured. The electrodes in dark blue are the ones activated in each example. The measured wave fronts are color coded with the scale given in micrometers. The surface's wave fronts are expressed as Zernike's polynomial expansion with 21 terms, which corresponds to the fifth order. As mentioned above, the influence functions are grouped in the IFM by columns. The dimensions of matrix IFM are 21×37, the number of Zernike modes and the number of electrodes.

#2380 - $15.00 US Received April 10, 2003; Revised April 25, 2003

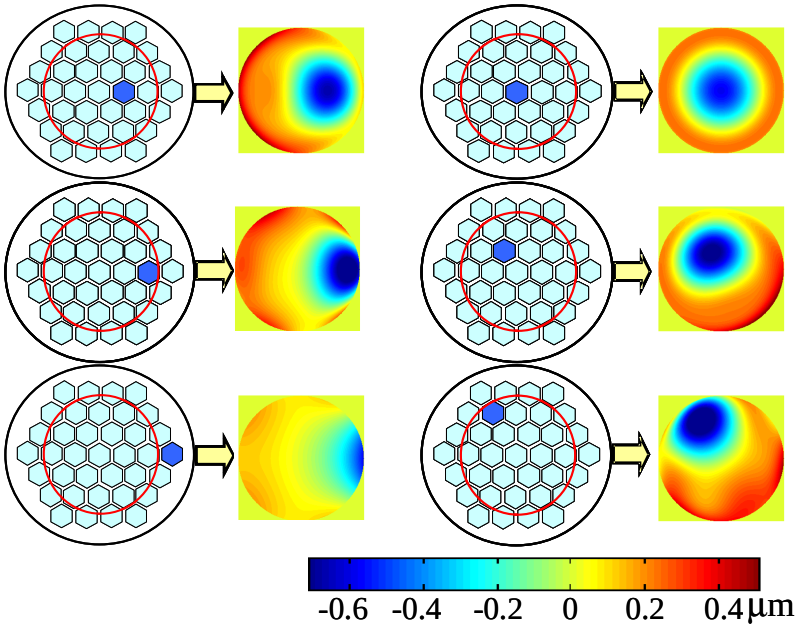

Fig. 2. Influence functions produced by the action of each isolated electrode over the membrane. The electrode structure underneath the deformable mirror and the 9.2 mm of diameter pupil on the membrane are presented. The deformation of the membrane is shown with a color-coded representation together with the corresponding electrode in dark blue.

4. Results

4.1. Mirror performance

To study the capabilities of the mirror, it is first necessary to solve Poisson equation (6), which describes the surface response. This can be done experimentally by means of the preceding setup, measuring the membrane profile with the Hartmann–Shack wave-front sensor. Equation (6) can be also solved mathematically. Both methods are used and discussed below.

To evaluate the mirror surface, we first developed a method based on the finite elements to solve Poisson equation (6). The electrodes were modeled as hexagons with the size ratio kept with the total mirrored area. The parameters describing the physical properties of the membrane and dimensions of the device were fitted from the values given by the mirror manufacturer. For accurate adjustment of all the parameters, they were fitted to produce a maximum deflection of the membrane of 8 μm in response to the action of all the electrodes. Once the model was calibrated, the influence functions were computed and grouped in the IFM. As long as the functions are obtained numerically, there is no truncation produced by the use of the Zernike polynomials. These polynomials are used in putting together the functions in the matrix, with use of up to the eighth order to minimize truncation.

From the registered IFM we computed the spatial modes of the membrane as discussed in Section 3. Each mode is associated with a nonzero singular value and represents the membrane's surfaces that the mirror produces perfectly. Figure 3 shows some selected modes of the mirror.

#2380 - $15.00 US
Received April 10, 2003; Revised April 25, 2003

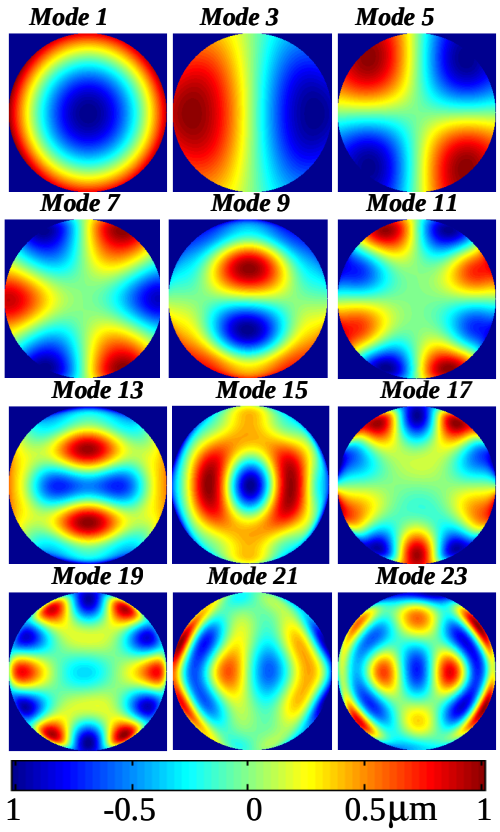

Fig. 3. Representative spatial modes of the deformable mirror. Any linear combination of them can theoretically be induced on the membrane.

They have been ordered so that higher modes correspond to larger singular values. Higher modes reproduce higher spatial details, but their peak-to-valley values remain similar throughout (see the range of colors in the Fig. 3). Because of the limited range of voltages that can be applied, some of these surfaces can be reproduced only within a small range. These types of modes are the natural choice to be eliminated from the standpoint of practical use, considering that a smaller number of modes in the matrix make the mirror control more robust. In this context, singular values smaller than 0.05 were truncated to zero in the experiment. Although the basis of spatial modes is useful for understanding the behavior of the membrane, it is not the best choice for expressing the measured wave fronts.

Each deformable mirror has its own particular modes depending on the shape, number, and distribution of the actuators and the elastic parameters of the membrane. However, the geometry of the problem suggests the use of Zernike's polynomials to represent the wave fronts over circular pupils. The problem then reduces to a usual change of basis from the membrane modes to the Zernike's polynomials. There is another important issue with the spatial modes based on the capability of the system to measure them. The employed Hartmann–Shack sensor will recover the wave aberration up to the fifth order, so very high spatial frequencies cannot be sensed. There is no reason to handle surface profiles that the system cannot measure. On the other hand, these modes can produce effects that are

#2380 - $15.00 US
Received April 10, 2003; Revised April 25, 2003

undetectable for the sensor, so an additional channel is necessary for checking the performance, as is discussed in below. Because of the finite number of membrane modes, not every Zernike polynomial can be exactly represented by the mirror; i.e., by a combination of

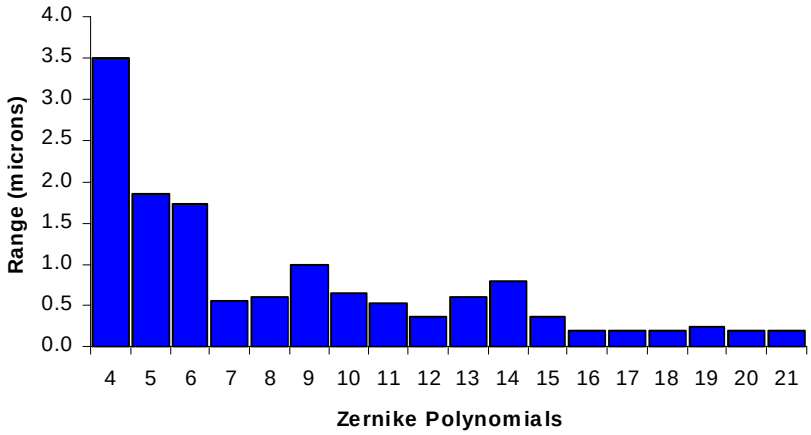

Fig. 4. Range of production of the Zernike coefficients for the 21st polynomials in the 9.2-mm-diameter pupil on the deformable membrane.

the mirror's modes. By use of the CM, the required set of voltages to produce each Zernike mode is obtained. Then the voltages are multiplied by the IFM to recover the closest surface, discussed in Section 2, to the required mode.

Figure 4 shows the range of production of the Zernike coefficients for the 21st first polynomials by the mirror. According to the preceding discussion, only the 12th first spatial modes were used, and this will be the chosen set of modes for the practical control. The ordering of the Zernike modes proposed by Noll [16] is used in Fig. 4 as well as in the rest of this paper. Piston and tilts, Zernike's modes 1–3, were not included. If the desired stroke of a particular Zernike mode grows, some of the nominally required voltages will be out of range. This is why, for robust operation of the mirror, the range of production of the Zernike modes needs to be within the levels of Fig. 4. These values were obtained considering that a particular mode is well reproduced if the error between the desired and the produced values was less than 0.1 μm on the pupil of 9.2-mm diameter. The range shown in Fig. 4 does not account for the sign of the Zernike coefficient but represents absolute values. In other words, each mode can be generated by the membrane in half the given range in both directions. The fourth coefficient, defocus, is induced the best, whereas higher orders of modes are produced less effectively. However, trefoil terms, 9 and 10, are better produced than coma, terms 7 and 8, despite their higher order. In the same direction, spherical aberration, the 11th term is not produced as well as the 14th.

Once the generation of the 21st Zernike modes by the mirror has been described, the same procedure can be applied to any desired surface. Figure 5 shows examples for some surfaces: the required shape, the residual surface (the difference between the desired and the obtained surfaces), and a schematic representation of the employed voltages in the electrodes.

#2380 - $15.00 US Received April 10, 2003; Revised April 25, 2003

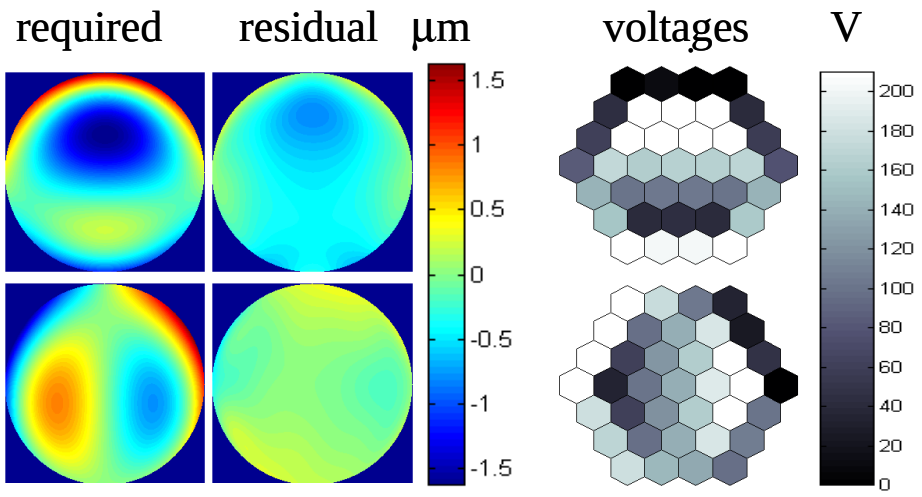

Fig. 5. Examples of the membrane's capability to reproduce some arbitrary surfaces. The required surface, at the top left side, is described by Zernike polynomials as Z_4 = 0.3 μm, Z_7 = 0.4 μm, and the rest of the coefficients equal to zero. The corresponding residual, at top center, is 0.16 μm. The voltage distributions on the electrodes underneath to produce the desired shape on the mirror are also shown. At the bottom the required surface is described by Z_5 = 0.2 μm, Z_8 = 0.3 μm, and the other coefficients equal to zero. The obtained residual was 0.8 μm in this case.

Once the method has provided a limit to the performance of the mirror, a procedure for controlling it can be evaluated. The functions were consecutively measured by the Hartmann–Shack sensor and then grouped in matrix IFM. To drive the mirror, the procedure to induce surfaces is applied iteratively. This permits achieving better performance than in a single iteration, thanks to the non-linearity effects. These effects can be induced in the system either by the wave-front sensing errors or as a result of overshooting in the applied voltages. The set of 37 voltages $\mathbf{V}(t_{k+1})$ at instant t_{k+1} is given by

$$\vec{V}(t_{k+1}) = \beta \cdot CM \cdot \left(\vec{S}_{req.} - \vec{S}_{measur.}(t_k)\right) + \vec{V}(t_k), \qquad (7)$$

Where vector $\mathbf{S}_{req.}$ is the required final surface to be produced by the mirror and $\mathbf{S}_{measur.}(t_k)$ is the measured surface's shape at previous instant t_k. These are the vectors of the Zernike's coefficients describing each surface. The vector $\mathbf{V}(t_k)$ is the current set of driving voltages, CM is the control matrix, and parameter β is a positive number between 0 and 1 accounting for the convergence rate. An adequate value of β as 0.35, empirically determined, notably enhances the accuracy and stability of the iterative control process. Higher values of β reduces the number of iterations, but convergence is worse. On the other hand, smaller β increases the number of iterations and the accuracy and stability of the process but at the cost of longer convergence times that are not adequate for real-time applications. Our choice of 0.35 is intended to be a compromise between precision and convergence time. The algorithm also uses limits for the available range of Zernike polynomials. The Zernike terms are programmed within the limits imposed by Fig. 4. The algorithm stops the iterations when any polynomial reaches the calculated limit. This procedure gives additional stability in the convergence. Figure 6 shows four examples of iterative generation of Zernike modes (Z_4,

#2380 - $15.00 US
Received April 10, 2003; Revised April 25, 2003

defocus; Z_5, astigmatism; Z_8, coma, and Z_{11}, spherical aberrations). The induced coefficients as a function of time are represented. The dotted horizontal curves are the target level of required aberration: –1, –0.5, 0.4, and 0.3 μm for modes Z_4, Z_5, Z_8, and Z_{11}, respectively, in a mirror's pupil diameter of 9.2 mm.

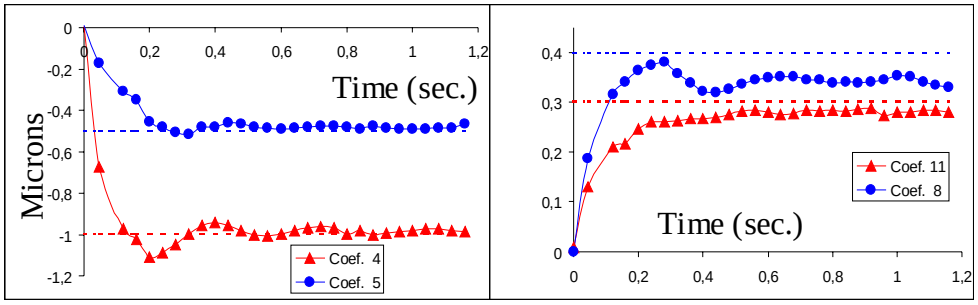

Fig. 6. Iterative generation of some Zernike polynomials as a function of time performed by the deformable mirror. The membrane's pupil is 9.2 mm in diameter. Points in the curves are 0.04 ms apart. The dotted horizontal curves are the programmed level of aberration in micrometers.

Four iterations, corresponding to 0.16 s, are required for approximately reaching the desired value that remains stable after induction. The measured coefficients after generation are: –0.98, -0.45, 0.32 and 0.28 μm for each mode (to be compared with the target values above).

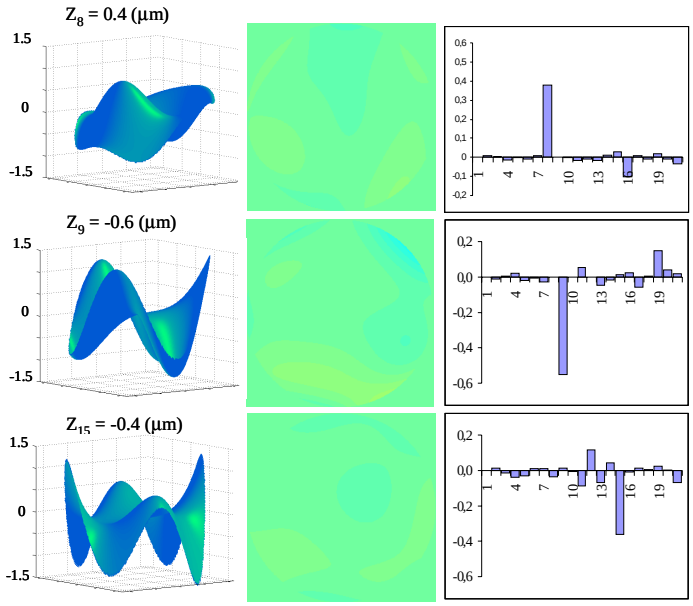

(a) (b)

Fig. 7. (a) Surfaces obtained by the deformable mirror. Some individual Zernike polynomials are replicated with programmed values of Z_8 = 0.4 μm, Z_9 = –0.6 μm, and Z_{15} = –0.4 μm. The pupil was 9.2 mm in diameter for the three cases. The final measured values were Z_8 = 0.32 μm, Z_9 = –0.56 μm, and Z_{15} = –0.34 μm, keeping the other coefficients less than 0.1 μm respectively. (1.14, 1.15, and 1 MB, respectively) Videos of the wave fronts during the generations are also shown in the next column[[?]]. (b) Final surfaces obtained in the preceding generations in terms of Zernike's polynomials in micrometers.

Figure 7 (a) presents another example of the dynamic generation of three Zernike modes by the mirror. The left-hand side shows the two-dimensional (2D) representation of the obtained modes; the right-hand side, the videos of the evolution of the wave front during the generation. In this example the target coefficients were 0.4, –0.6, and –0.4 μm for $Z_{8,}$ Z_9, and Z_{15}, respectively, and the values actually produced were 0.32, –0.56, and –0.34 μm (see the video clips as an example of Zernike mode production by the mirror). Figure 7 (b) shows the final values of the Zernike coefficients of the actual surfaces produced by the mirror. In some cases, the coupling among modes may be significant. This is a limitation for this type of mirror when pure Zernike's polynomials are required. In addition, it is also possible that, in some cases, unwanted higher-order modes beyond the precision of our wave-front sensor could be produced.

4.2. Use of the membrane mirror for closed-loop correction of the eye's aberration

In this section we present results of using the membrane deformable mirror to correct ocular aberrations. Some preliminary results of closed-loop correction and generation were presented elsewhere [10,24]. A more detailed analysis of the pros and cons of this technology for AO in the human eye is included here.

According to the reciprocity principle, the compensation of the wave aberrations consists of the conjugation of the received complex amplitude. The deformable mirror performs the compensation of only the phase, leaving the amplitude uncorrected. This effect can be neglected if the amplitude modulation is assumed to be small. The procedure for correcting ocular aberrations is as follows: (i) The subject's pupil is aligned with the deformable mirror by means of bite-bars to ensure a correct and stable centering; (ii) defocus is removed from the system by means of the computer-controlled motorized optometer working in closed-loop. This permits us to dedicate most of the mirror's stroke to correcting higher-order aberrations. (iii) Correction of the higher order aberrations in real time is performed with the membrane mirror. While the aberrations are corrected in real time, the subject can perform visual tasks or the retina can be imaged through the compensated optics.

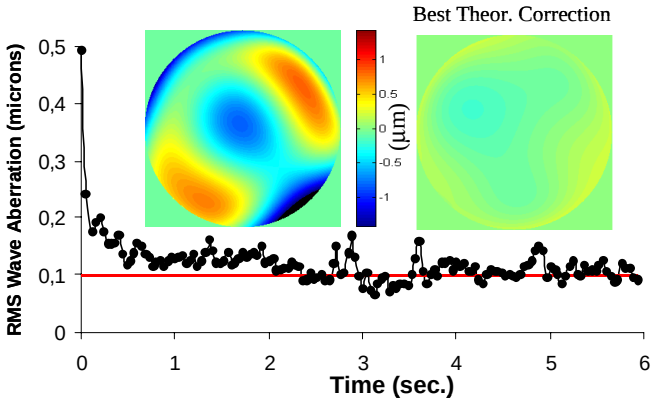

Fig. 8. Closed-loop aberration correction in the living eye by use of the deformable mirror. The evolution for the rms of the wave front through 6 s during the real-time compensation is shown. The red line corresponds to the best estimated compensation (0.098 μm). The eye's pupil studied was 5.52 mm in diameter under natural viewing conditions. Both the initial and the predicted best wave aberration correction are also shown in a color-coded representation.

An important factor in applying AO is the temporal bandwidth. In the case of the eye, both defocus and higher-order aberrations change over time even under stable experimental conditions [9]. However, most of the temporal power spectrum of the ocular aberration lies at

#2380 - $15.00 US
Received April 10, 2003; Revised April 25, 2003

temporal frequencies lower than 2–3 Hz. The system operates at 25 Hz and, as shown above, the mirror takes around 0.16 s to produce a required surface, which corresponds to a temporal bandwidth of 6 Hz. This renders the system appropriate for use in aberration compensation in the eye, probably in most cases of practical interest. It must be noted that the temporal limitations are due to the measuring and control procedures and not to the mirror temporal bandwidth.

Figure 8 shows an example of real-time closed-loop aberration correction in the eye of one of the authors (P. Artal) under natural viewing conditions for a pupil diameter of 5.5 mm. The plot (black symbols) shows the evolution of the rms of the eye aberration during the compensation process. The average value of rms in the closed–loop correction is 0.11 μm, to be compared with the initial rms value of 0.5 μm before correction. The rms value of the calculated best correction, as the surface that minimizes the residual, for the initial aberration pattern is 0.098 μm (red horizontal line in the Fig. 8). The video clip of the evolution of the eye's wave aberration during the compensation, together with the associated point-spread function (PSF), are presented in Fig. 9. The frames of the final part of the video clip are quite similar to the simulated best correction. This suggests that for this particular case, the performance of the adaptive system is quite close to its optimum. Many experimental factors contribute to less-than-adequate performance of the system in other cases: poor stability of the eye, blinking, movements, and the like.

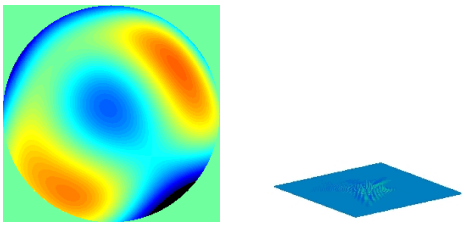

Fig. 9. (1.56 MB, 1.46 MB) Video of the measured wave aberration along the compensation together with the evolution of its associated PSF.

AO systems may have internal inconsistencies; i.e., it is possible to assume that the system perfectly corrects the aberrations, when this is not the case. This may happen, for instance, if the wave-front sensor has a systematic error. Then the influence functions for the membrane would be obtained with that bias, and the global failure of the system would not be noticeable only from the wave-front data. To be completely sure of the performance of our AO system, we set an additional path after the mirror: an additional video camera to record double-pass images of the point source in the retina.

Figure 10 shows retinal images with and without AO correction of the ocular aberrations also in the eye of one of the authors (P. Artal). The images on the top are calculated from the wave-front estimates (marked HS in Fig. 10). On the bottom, the double-pass retinal images in the same subject as recorded by the auxiliary camera under the same conditions are presented. To reduce speckle noise in the images, an average of six frames is presented. The recorded images are also represented as three-dimensional (3D) plots. On the one hand, the overall agreement in shape and size of these images provides a strong indication that our system is free of internal inconsistencies. It must be noted that the images computed from the aberrations are single-pass retinal images, whereas the experimental images are double-pass images [19]. On the other hand, the comparison between the recorded retinal images with and without AO shows an intensity enhancement at the central peak of nearly threefold,

#2380 - $15.00 US
Received April 10, 2003; Revised April 25, 2003

which further validates that we properly corrected most of the eye's aberrations. The approximate Strehl ratios obtained from the double-pass images were 0.45 and 0.16 for the compensated and the normal image, respectively.

The images estimated from Hartmann–Shack measurements do not indicate by themselves whether the system is performing the correction properly. Several factors contribute to this statement. First, the sensor does not take into account amplitude variations of the wave front. In addition, the aberrations are fitted only up to the fifth order. The mirror can produce, at least theoretically, spatial modes that require higher order to be correctly represented. Even though they have been suppressed of the control zeroing the corresponding singular values, this does not ensure that they can appear during the membrane operation. It is then essential that the additional double-pass retinal images be used to validate the procedure.

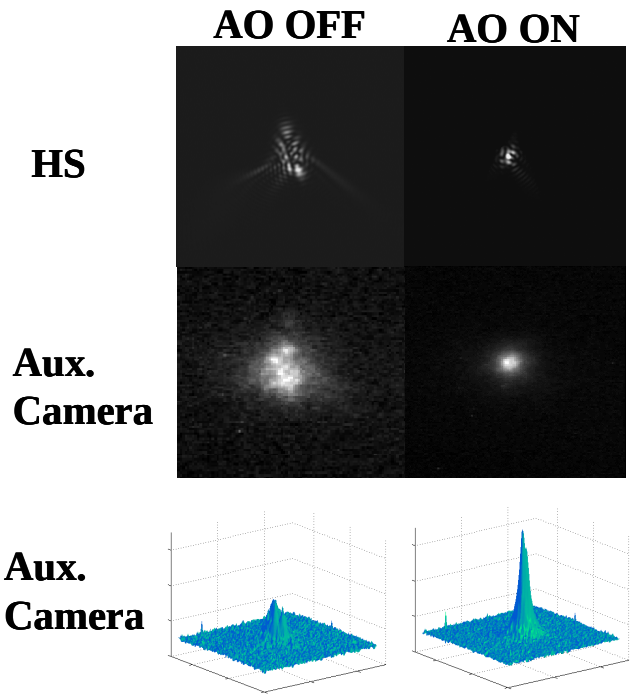

Fig. 10. Retinal images with and without AO. The eye pupil studied was 5.52 mm in diameter under natural viewing conditions. At the top, estimated PSF from the Hartmann–Shack measurements are presented. The retinal images recorded with the auxiliary camera are shown below. To compensate the speckle effects, six frames were added to obtain these figures. At the bottom, the 3D representation of the recorded images in arbitrary units (A.U.) is shown. The increment in intensity at peak maximum is 2.86 times during AO aberration correction.

5. Conclusions

We have used a powerful method to evaluate the capabilities of a membrane deformable mirror to produce and correct different aberrations within the range of interest in visual optics applications. The procedure has been applied systematically to produce both Zernike's polynomials and arbitrary surfaces, taking into account the available range of voltages in the device. This is a general approach, suitable for use in every system whose control was based on previous knowledge of its influence functions. Under the assumption of linearity, the

#2380 - $15.00 US
Received April 10, 2003; Revised April 25, 2003

proposed iterative algorithm works with adequate precision after a few iterations, making it appropriate for use in real-time applications. The robustness of the control method permits the convergence of the membrane to the required shape in approximately four iterations. In addition, the possibility of estimating the closest surface that the required the mirror can reach provides a test for evaluating the quality of the control procedure. The device has been incorporated into a real-time (25 Hz) closed-loop AO prototype for the compensation of ocular aberration. The system was able to perform partial correction of the ocular aberration at 6 Hz. The simultaneous recording of aerial images has prevented internal inconsistencies, otherwise undetectable in the method. The results indicate that the correction is performed properly, validating the control method. The inclusion of this AO apparatus in ophthalmoscopes could enhance both the resolution and the contrast of the images, aiding medical diagnosis. In addition, the proposed prototype can be used as a visual testing station, where the subject may perform different visual tasks through the required aberrations pattern.

Acknowledgments

This research was supported by MCyT, Spain (grant BFM2001-0391) and Pharmacia_Groningen, The Netherlands.

#2380 - $15.00 US Received April 10, 2003; Revised April 25, 2003